

Vertical optical transitions of helical Majorana edge modes in topological superconductors

Han Bi¹ and James Jun He^{2,*}

¹*International Center for Quantum Design of Functional Materials (ICQD),
Hefei National Research Center for Interdisciplinary Sciences at the Microscale,
University of Science and Technology of China, Hefei, Anhui 230026, China*

²*Hefei National Laboratory, Hefei, Anhui 230088, China*

 (Received 21 November 2023; revised 4 May 2024; accepted 20 May 2024; published 17 June 2024)

The search for evidence of Majorana states on the edges of topological superconductors is challenging due to the difficulty of detecting such charge-neutral electronic quasiparticles. Local microwave spectroscopy has been shown to be a possible method to detect propagating Majorana modes, where a spatially focused light beam must be used. Here, we show that helical Majorana modes in topological superconductors contribute to the optical conductivity under a spatially uniform light. The existence of such a signal requires the system to break certain symmetries so that the projection of charge current operator onto helical Majorana edge states leads to interbranch hybridization terms. The general form of this contribution under a tunable time-reversal breaking field is obtained, which is valid in the subgap low-frequency regime where the edge energy spectrum is linear. In comparison, the current operator for normal helical edge states, such as in quantum spin Hall insulators, does not cause interbranch transitions and the related optical conductivity vanishes unless the time-reversal symmetry is broken. Our results may help guide feasible experiments to provide evidence of Majorana edge modes in topological superconductors.

DOI: [10.1103/PhysRevB.109.214513](https://doi.org/10.1103/PhysRevB.109.214513)

I. INTRODUCTION

The search for Majorana modes in condensed matter physics [1–9] has been a critical and challenging problem. Such quasiparticles are believed to exist in topological superconductors (TSCs) where they may show up as one-dimensional (1D) propagating modes as well as zero-dimensional bound states.

Various systems have been predicted to host propagating helical [10–22] or chiral [23–31] Majorana modes with or without time-reversal symmetry, respectively. There have been experimental results [32–34] consistent with propagating-Majorana scenarios, but conclusive evidence of such exotic states in TSCs is yet to be achieved. The difficulties not only exist in experimental techniques but also in theoretical principles to interpret or predict Majorana signals. Despite possessing nonzero velocity, propagating Majorana modes do not carry any charge because their particles and antiparticles are identical [1]. The neutrality makes the detection of Majorana edge modes in TSCs much harder than normal edge states.

Strictly speaking, however, the neutrality is true only on average since Majorana modes alone do not preserve the U(1) gauge symmetry. This makes it possible for them to couple with external electromagnetic field, leading to particular optical responses that may serve as evidence of chiral Majorana modes [35,36]. In this case, translation symmetry needs to be strongly broken to see the predicted optical signal due to the absence of vertical optical transition. As a result, a

highly focused light beam, such as in microwave impedance microscopy [37], is required.

Here, we show that, without breaking the translational symmetry along the edge, the microwave absorption of helical Majorana modes (HMMs) in time-reversal invariant TSCs is nonzero and may be used as an effective detection method. We begin with a generic discussion with an effective theory containing only the edge states. The edge current operator, which should be a projection of the bulk current operator onto the edge states, is directly written down by physical arguments at this stage. A general form of the optical absorption is obtained, which is a result of the transition processes where a Cooper pair is broken into two Majorana modes that propagate in opposite directions. Such processes are vertical transitions from holes to electrons in the Nambu basis. Then we investigate this phenomenon in several models of TSCs supporting HMMs, including $p \pm ip$ -wave superconductors, topological insulator (TI) thin films in proximity to superconductivity, and doped quantum spin Hall (QSH) insulators, with or without perturbations that break the time-reversal symmetry. We show that they all share the same features predicted by the effective edge theory in the subgap low-energy region where the optical transitions happen among the Majorana edge states whose dispersion relations are approximately linear.

II. EFFECTIVE EDGE THEORY

A minimal theory of the helical Majorana edge states of a time-reversal invariant TSC may be described by the following Hamiltonian [10],

$$\mathcal{H} = \sum_{-k_0 < k < k_0} \Gamma_k^\dagger (vk\sigma_3 + M\sigma_2)\Gamma_k, \quad (1)$$

*jun_he@ustc.edu.cn

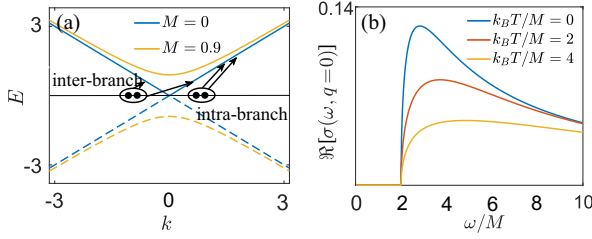


FIG. 1. (a) The energy spectra of the helical Majorana modes with ($M = 0$) and without ($M \neq 0$) time-reversal symmetry. Here the involving two bands correspond to opposite Fermi velocity $\pm v$ at $M = 0$. Intra-branch and interbranch optical transitions are schematically shown where Cooper pairs are broken into two Majorana modes. (b) The real-part homogeneous optical conductivity, $\Re[\sigma(\omega, 0)]$, as a function of the frequency ω given by Eq. (4).

where $\Gamma_k = [\gamma_{1k}, \gamma_{2k}]$ denotes the edge HMMs with $\gamma_{1/2}$ being the left-/right-moving branch. $\sigma_{1,2,3}$ are the Pauli matrices, k_0 is the momentum cutoff, and M is a time-reversal breaking term that opens a gap in the 1D spectrum. Generally, the momentum cutoff k_0 in Eq. (1) originates from an energy cutoff $\Delta = vk_0$ which corresponds to the topological gap of a TSC. This gap is usually smaller than the SC gap and is often of the order of 0.1 meV, corresponding to microwave. When $M = 0$, one readily finds that the time-reversal symmetry $\mathcal{T} = i\sigma_2\mathcal{K}$ and the particle-hole symmetry $\mathcal{P} = \mathcal{K}$ are both preserved. When $M \neq 0$, the energy eigenvalues are $\pm\xi_k$ with $\xi_k = \sqrt{(vk)^2 + M^2}$, which has a gap of M , as shown in Fig. 1(a).

The corresponding current density operator $j(x)$ is more conveniently written down in the real space. Considering its sign flip under both \mathcal{T} and \mathcal{P} , applying the Majorana algebra $\{\gamma_i(x), \gamma_j(x')\} = \delta_{ij}\delta(x - x')$, and keeping up to the first-order spatial derivative, one obtains the only possible form

$$j(x) = -ia(\gamma_1\partial_x\gamma_1 + \gamma_2\partial_x\gamma_2 - h.c.) - ib\gamma_1\gamma_2, \quad (2)$$

where a and b are real. Terms similar to $\gamma_1\partial_x\gamma_2$ are absent due to the Majorana commutation relations. And the term proportional to b may exist due to spin-orbit coupling (SOC).

The current operator in the momentum space is given by Fourier transformation $j_q = \int j(x)e^{-iqx}dx$ and the optical conductivity is given by the Kubo formula,

$$\Re[\sigma(\omega, q)] = \frac{1}{\omega L} \Im \int_0^{k_B T} d\tau e^{i\omega\tau} \langle T_\tau j_{-q}(\tau) j_q(0) \rangle, \quad (3)$$

with \Re (\Im) denoting the real (imaginary) part. L is the system length, k_B is the Boltzmann constant, T is the temperature, ω is the frequency, τ is the imaginary time, and q is the transferred momentum during a photon absorption. For a uniform detecting light, we only need to consider the $q = 0$ component. Equation (3) is calculated using Wick's theorem and Mastubara Green's function, yielding

$$\Re[\sigma(\omega, 0)] = \frac{b^2}{4v\omega^2} \sqrt{\omega^2 - (2M)^2} \tanh \frac{\omega}{2k_B T}. \quad (4)$$

When the temperature $T \rightarrow 0$ and $M = 0$, the $\Re[\sigma(\omega, 0)]$ curve decreases as $1/\omega$. For nonzero M , $\Re[\sigma(\omega, 0)]$ vanishes when $\omega < 2M$, which is the lowest energy to break a Cooper pair into two edge states with the same energy and

opposite momenta. $\Re[\sigma(\omega, 0)]$ reaches the maximum value at $\omega = 2\sqrt{2}M$ and decreases with further increasing ω , as shown in Fig. 1(b).

Note that the right-hand side of Eq. (4) vanishes if $b = 0$, and thus the last term in Eq. (2) is crucial for the interbranch transitions. This term has been taken for granted up to now. In the following, we study concrete TSC models where the interbranch term of $j(x)$ appears by breaking the inversion symmetry.

III. $p \pm ip$ SUPERCONDUCTORS

As the simplest case, let us first consider a $p \pm ip$ -wave TSC described by the following Hamiltonian [38]:

$$H_{p \pm ip} = \left(\frac{\hbar^2 k^2}{2m} - \mu \right) \tau_3 \sigma_0 + A_p (k_x \tau_0 \sigma_1 + k_y \tau_3 \sigma_2) + \Delta_p (k_x \tau_1 \sigma_0 - k_y \tau_2 \sigma_3), \quad (5)$$

with the basis $\Psi^\dagger(\mathbf{k}) = [\psi_{k\uparrow}^\dagger, \psi_{k\downarrow}^\dagger, \psi_{-k\uparrow}, \psi_{-k\downarrow}]$. Here τ and σ are Pauli matrices acting on the particle hole and spin degrees of freedom, respectively. A pair of gapless helical Majorana states appear at the boundary of the 2D system and are protected by the time-reversal symmetry \mathcal{T} , which can be broken by a small Zeeman term $H_z = B_p \tau_3 \sigma_1$. The spin-orbit coupling term proportional to A_p is necessary in order to induce optical response to a uniform light, because the Hamiltonian (5) with $A_p = 0$ commutes with the spin operator σ_3 and there is no mixing between \uparrow and \downarrow , indicating $b = 0$ in Eq. (2) and thus vanishing vertical transition. Note that an edge gap can be opened by a Zeeman field in an arbitrary direction when SOC is present, unlike in the case of Majorana Ising spin [39–42].

In the following, we calculate the optical absorption on the edges with the light linearly polarized along the edge. The relevant current density operator is

$$j_x = \begin{pmatrix} j_n(\mathbf{k}) & \\ & -j_n^T(-\mathbf{k}) \end{pmatrix}, \quad (6)$$

where $j_n(\mathbf{k}) = ek_x/\hbar\sigma_0 + A_p\sigma_1$ is the k derivative of the normal state Hamiltonian $H_n = (\hbar^2 k^2/2m - \mu)\sigma_0 + B_p\sigma_1 + A_p \mathbf{k} \cdot \boldsymbol{\sigma}$. We take open boundary conditions along the y direction while k_x remains a good quantum number. The Kubo formula calculated in the energy eigenstate basis under uniformly distributed detecting light becomes

$$\sigma(\omega) = \frac{i\hbar}{\Omega} \sum_{k_x, m, n} \frac{|\langle nk_x | j_x | mk_x \rangle|^2}{\xi_{mk_x} - \xi_{nk_x}} \frac{f(\xi_{nk_x}) - f(\xi_{mk_x})}{\hbar\omega + \xi_{nk_x} - \xi_{mk_x} + i\eta}, \quad (7)$$

with Ω the area of the shining light, ξ_{nk_x} the eigenenergy of the eigenstate $|nk_x\rangle$, $\eta \ll \Delta_p$ a small real constant, and $f(\xi)$ the Fermi distribution function. At low temperatures, we get the δ function $\delta(\hbar\omega + \xi_{nk_x} - \xi_{mk_x})$, revealing the energy conservation during the optical process. Note that, in the absence of SOC effect, j_x is proportional to the identical matrix and no interbranch transition occurs due to the orthogonality of $|nk_x\rangle$ and $|mk_x\rangle$. Adding SOC terms breaks the inversion symmetry and produces spin-mixing terms in the current operator. Then, we expect nontrivial interbranch transition described by the effective 1D theory in the previous section.

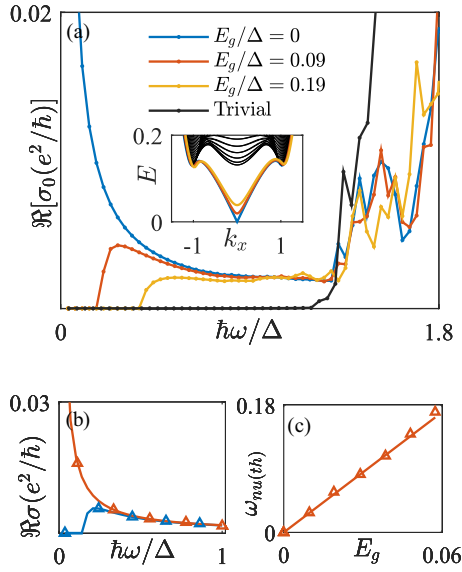


FIG. 2. (a) The frequency dependence of optical conductivity for various values of the edge gap E_g . The common parameters: pairing amplitude $\Delta = 0.2$, SOC strength $A_p = 0.05$, mass term $m = 1$, chemical potential $\mu = 0.5$, and $k_B T = 10^{-4}$. k_B is the Boltzmann constant. The inset shows the corresponding energy spectra. (b) The numerical (dots) and the analytical [lines, obtained with Eq. (4)] of the real-part conductivity for both the time-reversal invariant (red) and the time-reversal broken case (blue). (c) The corresponding peak position $\omega_{nu(th)}$ where the real-part conductivity reaches its maximum under various values of E_g .

Figure 2(a) shows the real-part conductivity $\Re[\sigma(\omega)]$ obtained numerically. When the Zeeman field $B_p = 0$, the optical absorption induced by the in-gap HMMs diverges as $\omega \rightarrow 0$. This is in agreement with the prediction of the effective theory in which $\Re[\sigma(\omega)] \sim 1/\omega$. For nonzero but small B_p , the edge states acquire a gap, denoted by E_g . Thus, there is no absorption for $\omega < 2E_g$ unless thermal excitation from finite temperature effects. $\Re[\sigma(\omega)]$ rapidly increases near $\omega > 2E_g$ and reaches a maximum at $\omega_{nu(th)}$. It decreases as ω further goes up until it reaches the bulk gap, where the contribution of the bulk states dominates. For the topologically trivial phase, no optical response is observed inside the bulk gap. Figure 2(b) shows the real-part optical conductivity contributed by the edge states, with or without time-reversal symmetry, together with the corresponding analytical results of the effective 1D theory. Figure 2(c) shows the positions of the maximum $\Re[\sigma]$ for various values of the energy gap. They both show great agreement between the numerical and the analytical results.

The optical conductivity of the $p \pm ip$ -wave superconductor in response to a locally distributed detecting light is also studied by transforming Eq. (5) into a tight-binding model. The current density along the x direction is $j_x(\mathbf{r}) = \frac{ie\hbar}{2m} \psi_r^\dagger \psi_{r+\hat{x}} + A_p \psi_r^\dagger \psi_r + \text{H.c.}$ The vector $\mathbf{r} = x\hat{x} + y\hat{y}$ (x and y being integers, \hat{x} and \hat{y} being unit vectors along the x and y directions, respectively) denotes the position on a square lattice. The system is assumed infinite along the x direction but has a finite number of sites, L_y , along the y direction. The size of the detecting area is determined by the confinements

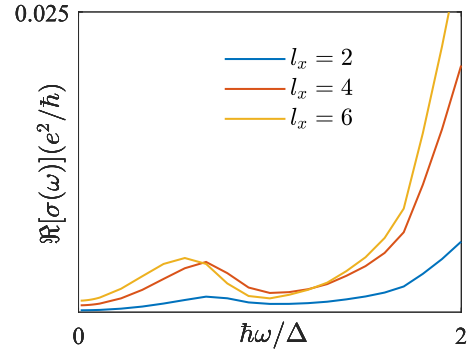


FIG. 3. The frequency dependence of the real-part local conductivity $\Re[\sigma_l(\omega)]$ of the $p \pm ip$ -wave superconductors system. The results for different values of the shining length l_x are plotted in different colors. Other related parameters are set to be the same to those in Fig. 2 with $E_g = 0$.

$1 \leq x \leq l_x$ and $1 \leq y \leq l_y$, where the integer l_y is chosen to cover the spread of the edge state wave functions. The current operator to calculate the optical response in the detecting area is obtained by confining the current operator to the shined region [35]

$$J_x = \frac{1}{l_x} \sum_{n_x=1}^{l_x} \sum_{n_y=1}^{l_y} j_x(\mathbf{r} + n_x\hat{x} + n_y\hat{y}). \quad (8)$$

Figure 3 shows the results for different shining lengths l_x obtained using the recursive Green's function method. For small l_x we get a similar shape of the $\Re[\sigma_l(\omega)]$ curve compared to the chiral case [35]. A major difference is the nonzero value of $\Re[\sigma_l(\omega = 0)]$, which is a consequence of the interbranch term ($\sim b$) in the current operator of Eq. (2). As l_x increases, the peak shifts toward a lower frequency and the peak height increases. For very large l_x , the result becomes similar to the uniform case, as expected since the limit $l_x \rightarrow \infty$ recovers uniformity.

IV. TI THIN FILM

The surface states of TIs can be used to design a time-reversal invariant TSC by proximity to conventional superconductors. If the SC order parameters induced on the two surfaces of a TI thin film are different by a phase π , a pair of HMMs appear on the edges [12,18]. With only the surface states considered, the normal state Hamiltonian can be written as

$$H_0^{\text{TF}}(\mathbf{k}) = 2A_r \tau_z \mathbf{d} \cdot \boldsymbol{\sigma} + m_k \tau_x \sigma_0 \quad (9)$$

under the basis $\Psi_{\mathbf{k}}^\dagger = [c_{\mathbf{k},+,\uparrow}^\dagger, c_{\mathbf{k},+,\downarrow}^\dagger, c_{\mathbf{k},-,\uparrow}^\dagger, c_{\mathbf{k},-,\downarrow}^\dagger]$, where \pm denotes the two surfaces. The vector $\mathbf{d} = [k_x, k_y, 0]$ and the function $m_{\mathbf{k}} = m_0 - t_f(k_x^2 + k_y^2)$. The first term of Eq. (9) describes the two Dirac cones located at the two surfaces and the second term represents the intersurface coupling. An inversion-symmetry-breaking term (originating from the substrate, for example) is needed to induce vertical optical transition [43,44], which may be, for example, a Rashba SOC on one surface,

$$H_R^{\text{TF}}(\mathbf{k}) = \alpha_{tf}(\tau_0 + \tau_z)\mathbf{d} \times \boldsymbol{\sigma}. \quad (10)$$

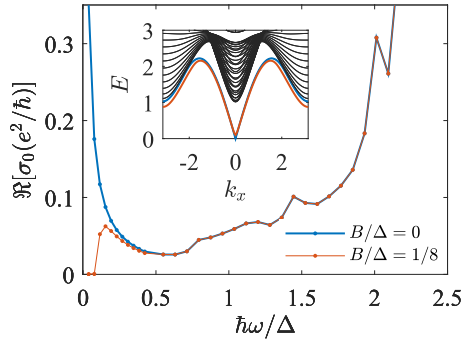


FIG. 4. The frequency dependence of the real-part conductivity of the HMMs in the TI thin film model given by Eqs. (9) and (10), with the parameters $A_t = 1$, $t_f = 1$, $\alpha_{tf} = 1$, $m_0 = 3$, and $\Delta = 2$. The inset is the energy spectrum where the edge states are highlighted by corresponding colors.

Equations (9) and (10) added by an s -wave pairing, $\Delta(\mathbf{k}) = i\Delta\tau_z\sigma_y$, form the total Hamiltonian. The sign difference of the order parameter between the upper and lower surfaces guarantees the time-reversal symmetry, which can be slightly broken by an external Zeeman field $H_z = B\tau_0\sigma_z$ or by a deviation from the exact π -phase difference.

Adding time-reversal breaking terms will open small gaps at these points. As shown in Fig. 4, the frequency dependence of the real-part conductivity near the $k_x = 0$ point (i.e., near $\omega = 0$) has a similar functional form to that of the $p \pm ip$ -wave TSCs and agrees with Eq. (4).

V. DOPED QSH INSULATOR

Quantum spin Hall insulators are proposed to be a TSC through correlation effects [15]. With this model system, one can directly compare the optical response of the HHMs to that of helical normal fermions, which could be achieved in different parameter regimes.

Consider the following Hamiltonian describing a QSH insulator [45]:

$$\mathcal{H}_0 = M(\mathbf{k})\sigma_0\tau_3 + A(k_x\sigma_3\tau_1 - k_y\sigma_0\tau_2), \quad (11)$$

where the Pauli matrices σ_i and τ_i ($i = 1, 2, 3$) act on the spin and orbital spaces, respectively. $M(\mathbf{k}) = m_0 - t(k_x^2 + k_y^2)$ and $m_0t > 0$ is required to guarantee the nontrivial topology of the normal state. It has been predicted that a TSC phase with $\Delta_{\mu\nu}^{12}(\mathbf{k}) = \Delta c_{1,k\mu}c_{2,-k\nu}\delta_{\mu\nu}$ is favored at certain doped regions with an inversion-breaking Rashba SOC [15],

$$\mathcal{H}_R = A_1(k_x\sigma_2 - k_y\sigma_1) \otimes (\tau_3 + \tau_0). \quad (12)$$

Here the subscript $\mu(\nu)$ labels the electron spins and the superscript 1(2) represents different orbitals.

The TSC phase has a pair of helical Majorana states propagating along the boundary, which is replaced by normal-fermion edge states when the pairing term vanishes and the system transforms into a QSH phase. In the presence of a time-reversal breaking term $\mathcal{H}_Z = Z\sigma_3\tau_0$, the edge states develop new features including a small gap, as shown in Figs. 5(c) and 5(d).

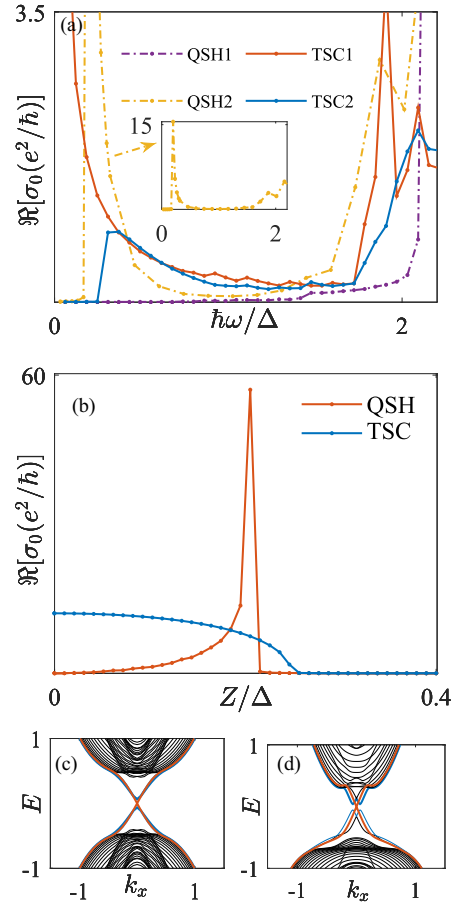


FIG. 5. (a) The frequency dependence of real-part conductivity of the doped QSH system in the QSH phase and in the TSC phase. For the TSC state the parameters are $A = 2$, $\Delta = 0.5$, $t = 2$, $m_0 = 0.1$, $A_1 = 2$, $Z = 0$ (for the red line), and $Z = 0.2$ (for the blue line). For the QSH state: $A = 2$, $\Delta = 0$, $t = 2$, $m_0 = 0.7$, $A_1 = 2$, $Z = 0$ (for the purple line), and $Z = 0.2$ (for the yellow line). (b) The real-part conductivity at fixed frequency $\omega_0^{\text{TSC}} = 0.15$ for the TSC phase and $\omega_0^{\text{QSH}} = 0.05$ for the QSH phase. (c) and (d) are the energy spectrum of the TSC phase and the QSH phase, respectively, where the time-reversal invariant (broken) edge states are in red (blue).

The frequency dependence of real-part conductivity for the TSC phase and the QSH phase are shown in Fig. 5(a), where the TSC results share similar features to the former TSC models, consistent with Eq. (4). The results for the QSH phase are rather different, with the optical conductivity inside the topological gap vanishing if $Z = 0$. When $Z \neq 0$, it has a sharp peak at $2E_g$, where E_g is the gap of the edge states. Above $2E_g$ it decreases as ω goes up. As another major difference between the TSC phase and QSH phase, the fixed-frequency responses with increasing external Zeeman field are shown in Fig. 5(b). For the TSC phase, $\Re\sigma_0$ at a fixed frequency ω_0^{TSC} keeps decreasing with increasing Zeeman field, reaching zero when $\omega_0 < 2E_g$. For the QSH phase, however, $\Re\sigma_0$ starts to increase from zero and reaches its maximum at $\omega_0^{\text{QSH}} = 2E_g$. Then it drops to zero sharply after $\omega_0 < 2E_g$.

The differences inside the bulk gap between the QSH phase and the TSC phase originate from the different mechanisms through which the edge states couple with electromagnetic

waves. While the light coupling of the HMMs relies on the bulk system and the corresponding current operator must be obtained by projecting the bulk version to the edges, the current operator of the QSH edge states may be directly derived within the effective edge theory which preserves the U(1) gauge symmetry. By introducing a gauge field to the edge theory, the current operator, $j_n \sim v(\psi_1^\dagger \psi_1 - \psi_2^\dagger \psi_2)$, can be readily obtained without referring to the bulk. It is simply the k derivative of the edge Hamiltonian $h_{edge}(k) = vk(\psi_1^\dagger \psi_1 - \psi_2^\dagger \psi_2)$. Following the same procedures in the previous effective 1D theory of Majorana edge states, we get the optical absorption for the QSH edge states at zero temperature, $\Re[\sigma_{QSH}(\omega)] \sim \omega^{-2}(\omega^2 - 4M^2)^{-1/2}$, where M is the edge gap opened by time-reversal symmetry breaking. Note that, besides the above major difference, the optical responses of the QSH edge states and the HMMs may happen in different ranges of wavelength since a QSH insulator may have a much larger topological gap.

VI. CONCLUSION AND DISCUSSION

We have demonstrated that helical Majorana modes induce microwave absorption. It originates from interbranch optical transition processes that are made possible by the broken U(1) gauge and spatial-inversion symmetries. The analytical form of the resulting optical conductivity is obtained with an effective edge theory, which is qualitatively confirmed by numerical calculations with several models of topological superconductors. The zero-temperature real-part optical conductivity $\Re[\sigma(\omega)]$ induced by the helical Majorana modes under uniform light is proportional to ω^{-1} . When the time-reversal symmetry is broken and an energy gap of M is opened on the edge, $\Re[\sigma(\omega)]$ has a maximum value at $\omega = 2\sqrt{2}M$. In comparison, vertical optical transitions in helical normal edge states in quantum spin Hall insulators are forbidden unless the time-reversal symmetry is broken after which the functional form of $\Re[\sigma(\omega)]$ becomes similar to that of Majorana modes. This difference originates from the different mechanisms of coupling with the U(1) gauge field.

Our results show that optical measurements may provide evidence of Majorana edge states in time-reversal invariant topological superconductors. Different from Ref. [35], the detecting light here is uniform and experiments will not encounter the difficulty of focusing a light beam into a tiny spatial region. A possible difficulty may come from the background optical absorption signal induced by the bulk Cooper pairs, which may be much larger than the edge-state contribution and make the Majorana signal hard to distinguish. One way to overcome this problem is to tune the external magnetic field which changes the functional form of the Majorana contribution qualitatively while its effect on the background signal is only quantitatively. In this way, it is possible to extract the Majorana contribution.

ACKNOWLEDGMENTS

J.J.H. is supported by the Innovation Program for Quantum Science and Technology (Grant No. 2021ZD0302800) and the National Natural Science Foundation of China (Grant No. 12204451).

APPENDIX: DERIVATION OF THE OPTICAL CONDUCTIVITY WITH THE EFFECTIVE EDGE THEORY

To illustrate the optical response of the HMMs, we start from the real space current operator $j(x) = j_a(x) + j_b(x)$ including both intrabranched and interbranched current. Unlike the normal electronic states where the current operator involves the coupling between fermionic modes and the external electromagnetic field, here $j(x)$ is obtained by projecting of the bulk current onto the edge states. By further considering the Majorana algebra, the surviving terms of $j(q) = \int dx j(x)e^{-iqx}$ only contains

$$j_a(q) = a \sum_k k(\gamma_{1,q-k}\gamma_{1,k} + \gamma_{2,q-k}\gamma_{2,k}), \quad (A1)$$

$$j_b(q) = -ib \sum_k \gamma_{1,q-k}\gamma_{2,k}. \quad (A2)$$

We define the current-current correlation $\Pi(q, \tau) = -\langle T_\tau j^\dagger(q, \tau)j(q) \rangle$, and we discuss the effects of both intrabranched and interbranched process denoted as a and b , respectively. Under the Fourier transformation $\Pi(i\omega_n) = \int_0^{k_B T} \Pi(q, \tau)e^{i\omega_n \tau}$, the correlation function in the frequency space at $T \rightarrow 0$ is given by

$$\begin{aligned} \Pi_a(i\omega_n) = & -a^2 \sum_k (2k^2 - kq)[\theta(k) - \theta(k - q)] \\ & \times \left(\frac{1}{i\omega_n + vq} + \frac{1}{i\omega_n - vq} \right), \end{aligned} \quad (A3)$$

$$\Pi_b(i\omega_n) = -b^2 \sum_k \frac{\theta(-k) - \theta(k - q)}{i\omega_n - 2vk + vq}. \quad (A4)$$

Thus, only the interbranched process contributes to the $q = 0$ optical response. According to Eq. (3), the corresponding optical conductivity is

$$\Re[\sigma(q = 0, \omega)] = \frac{b^2}{4\omega v}. \quad (A5)$$

We now generalize our calculation to the TRB case. The $q = 0$ current operator is given by

$$j(k) = ak\sigma_0 + b\sigma_3 \quad (A6)$$

under the basis $\Gamma_k^\dagger = [\gamma_{1,k}^\dagger, \gamma_{2,k}^\dagger]$. Under the Bogoliubov transformation we can diagonalize the 1D Hamiltonian $H \rightarrow \tilde{H} = UHU^\dagger$, $\Gamma^\dagger \rightarrow \tilde{\Gamma}^\dagger = [\tilde{\gamma}_1^\dagger, \tilde{\gamma}_2^\dagger]$. The current operator should become

$$\begin{aligned} \tilde{j}(k) = & ak\sigma_0 + b \begin{pmatrix} u_k & v_k \\ v_k^* & -u_k^* \end{pmatrix} \sigma_2 \begin{pmatrix} u_k^* & v_k \\ v_k^* & -u_k \end{pmatrix} \\ = & ak\sigma_0 + b \begin{pmatrix} i\Im(v_k u_k^*) & i(u_k^2 + v_k^2) \\ -i(u_k^{*2} + v_k^{*2}) & -i\Im(u_k^* v_k) \end{pmatrix} \end{aligned} \quad (A7)$$

in the new basis. To maintain the Majorana algebra of the new quasiparticle states $\{\tilde{\gamma}_{ik}^*, \tilde{\gamma}_{jk'}\} = \delta_{ij}\delta_{k,-k'}$ the parameters $u_k = |u_k|e^{i\phi_u}$, $v_k = |v_k|e^{i\phi_v}$ should satisfy $|u_k|^2 = \frac{1}{2} +$

$\frac{1}{2} \frac{\epsilon_k}{\xi_k}$, $|v_k|^2 = \frac{1}{2} - \frac{1}{2} \frac{\epsilon_k}{\xi_k}$, and $\phi_u - \phi_v = \frac{\pi}{2}$ where $\epsilon_k = vk$ and $\xi_k = \sqrt{\epsilon_k^2 + M^2}$.

The $ak\sigma_0$ term from Eq. (A7) does not contribute to the current-current correlation because it only involves terms like $\langle T_\tau \tilde{\gamma}_i^\dagger(\tau) \tilde{\gamma}_i(\tau) \tilde{\gamma}_i^\dagger \tilde{\gamma}_i \rangle$ ($i = 1, 2$). Such terms vanish under Wick's theorem since the involving Green's functions belong to the same Majorana operator. However, the second term of Eq. (A7) will cause connected diagrams

$$\Pi_{21}(\tau) = -4b^2 \sum_{k>0} |u_k^2 + v_k^2|^2 \langle T_\tau \tilde{\gamma}_{2k}^\dagger(\tau) \tilde{\gamma}_{1k}(\tau) \tilde{\gamma}_{1k}^\dagger \tilde{\gamma}_{2k} \rangle \quad (\text{A8})$$

to correspond to the interbranch transition. In the frequency space we have

$$\Pi_{21}(i\omega_n) = -b^2 \sum_{k>0} \frac{\epsilon_k^2}{\xi_k^2} \frac{f(\xi_k) - f(-\xi_k)}{i\omega_n - 2\xi_k}, \quad (\text{A9})$$

and the real-part optical conductivity is given by

$$\begin{aligned} \Re[\sigma(\omega)] &= -\frac{1}{\omega L} \Im[\Pi_{21}(i\omega_n)], \\ &= \frac{b^2}{4v\omega^2} \sqrt{\omega^2/4 - M^2} \tanh \frac{\omega}{2k_B T}. \end{aligned} \quad (\text{A10})$$

-
- [1] A. Y. Kitaev, Unpaired majorana fermions in quantum wires, *Phys. Usp.* **44**, 131 (2001).
- [2] F. Wilczek, Majorana returns, *Nat. Phys.* **5**, 614 (2009).
- [3] J. Alicea, New directions in the pursuit of Majorana fermions in solid state systems, *Rep. Prog. Phys.* **75**, 076501 (2012).
- [4] M. Leijnse and K. Flensberg, Introduction to topological superconductivity and Majorana fermions, *Semicond. Sci. Technol.* **27**, 124003 (2012).
- [5] C. Beenakker, Search for Majorana fermions in superconductors, *Annu. Rev. Condens. Matter Phys.* **4**, 113 (2013).
- [6] S. R. Elliott and M. Franz, Colloquium: Majorana fermions in nuclear, particle, and solid-state physics, *Rev. Mod. Phys.* **87**, 137 (2015).
- [7] E. Prada, P. San-Jose, M. W. de Moor, A. Geresdi, E. J. Lee, J. Klinovaja, D. Loss, J. Nygård, R. Aguado, and L. P. Kouwenhoven, From Andreev to Majorana bound states in hybrid superconductor–semiconductor nanowires, *Nat. Rev. Phys.* **2**, 575 (2020).
- [8] K. Flensberg, F. von Oppen, and A. Stern, Engineered platforms for topological superconductivity and Majorana zero modes, *Nat. Rev. Mater.* **6**, 944 (2021).
- [9] B. Jäck, Y. Xie, and A. Yazdani, Detecting and distinguishing Majorana zero modes with the scanning tunnelling microscope, *Nat. Rev. Phys.* **3**, 541 (2021).
- [10] L. Fu and C. L. Kane, Superconducting proximity effect and Majorana fermions at the surface of a topological insulator, *Phys. Rev. Lett.* **100**, 096407 (2008).
- [11] X.-L. Qi, T. L. Hughes, S. Raghu, and S.-C. Zhang, Time-reversal-invariant topological superconductors and superfluids in two and three dimensions, *Phys. Rev. Lett.* **102**, 187001 (2009).
- [12] C.-X. Liu and B. Trauzettel, Helical Dirac-Majorana interferometer in a superconductor/topological insulator sandwich structure, *Phys. Rev. B* **83**, 220510(R) (2011).
- [13] S. Deng, L. Viola, and G. Ortiz, Majorana modes in time-reversal invariant s -wave topological superconductors, *Phys. Rev. Lett.* **108**, 036803 (2012).
- [14] S. Deng, G. Ortiz, and L. Viola, Multiband s -wave topological superconductors: Role of dimensionality and magnetic field response, *Phys. Rev. B* **87**, 205414 (2013).
- [15] J. Wang, Y. Xu, and S.-C. Zhang, Two-dimensional time-reversal-invariant topological superconductivity in a doped quantum spin-Hall insulator, *Phys. Rev. B* **90**, 054503 (2014).
- [16] F. Yang, C.-C. Liu, Y.-Z. Zhang, Y. Yao, and D.-H. Lee, Time-reversal-invariant topological superconductivity in n -doped BiH, *Phys. Rev. B* **91**, 134514 (2015).
- [17] S.-J. Sun, C.-H. Chung, Y.-Y. Chang, W.-F. Tsai, and F.-C. Zhang, Helical majorana fermions in $d_{x^2-y^2} + id_{xy}$ -wave topological superconductivity of doped correlated quantum spin Hall insulators, *Sci. Rep.* **6**, 24102 (2016).
- [18] F. Parhizgar and A. M. Black-Schaffer, Highly tunable time-reversal-invariant topological superconductivity in topological insulator thin films, *Sci. Rep.* **7**, 9817 (2017).
- [19] A. Haim and Y. Oreg, Time-reversal-invariant topological superconductivity in one and two dimensions, *Phys. Rep.* **825**, 1 (2019).
- [20] R.-X. Zhang, W. S. Cole, and S. Das Sarma, Helical hinge majorana modes in iron-based superconductors, *Phys. Rev. Lett.* **122**, 187001 (2019).
- [21] R.-X. Zhang, W. S. Cole, X. Wu, and S. Das Sarma, Higher-order topology and nodal topological superconductivity in Fe(Se,Te) heterostructures, *Phys. Rev. Lett.* **123**, 167001 (2019).
- [22] R.-X. Zhang and S. Das Sarma, Intrinsic time-reversal-invariant topological superconductivity in thin films of iron-based superconductors, *Phys. Rev. Lett.* **126**, 137001 (2021).
- [23] N. Read and D. Green, Paired states of fermions in two dimensions with breaking of parity and time-reversal symmetries and the fractional quantum Hall effect, *Phys. Rev. B* **61**, 10267 (2000).
- [24] L. Fu and C. L. Kane, Probing neutral Majorana fermion edge modes with charge transport, *Phys. Rev. Lett.* **102**, 216403 (2009).
- [25] A. Akhmerov, J. Nilsson, and C. W. J. Beenakker, Electrically detected interferometry of Majorana fermions in a topological insulator, *Phys. Rev. Lett.* **102**, 216404(R) (2009).
- [26] X.-L. Qi, T. L. Hughes, and S.-C. Zhang, Chiral topological superconductor from the quantum Hall state, *Phys. Rev. B* **82**, 184516 (2010).
- [27] A. Daido and Y. Yanase, Majorana flat bands, chiral Majorana edge states, and unidirectional Majorana edge states in noncentrosymmetric superconductors, *Phys. Rev. B* **95**, 134507 (2017).
- [28] J. Wang and B. Lian, Multiple chiral Majorana fermion modes and quantum transport, *Phys. Rev. Lett.* **121**, 256801 (2018).
- [29] B. Lian, X.-Q. Sun, A. Vaezi, X.-L. Qi, and S.-C. Zhang, Topological quantum computation based on chiral Majorana fermions, *Proc. Natl. Acad. Sci. USA* **115**, 10938 (2018).

- [30] J. J. He, T. Liang, Y. Tanaka, and N. Nagaosa, Platform of chiral Majorana edge modes and its quantum transport phenomena, *Commun. Phys.* **2**, 149 (2019).
- [31] B. Fu, Z.-A. Hu, C.-A. Li, J. Li, and S.-Q. Shen, Chiral Majorana hinge modes in superconducting Dirac materials, *Phys. Rev. B* **103**, L180504 (2021).
- [32] Y. Kasahara, T. Ohnishi, Y. Mizukami, O. Tanaka, S. Ma, K. Sugii, N. Kurita, H. Tanaka, J. Nasu, Y. Motome *et al.*, Majorana quantization and half-integer thermal quantum Hall effect in a Kitaev spin liquid, *Nature (London)* **559**, 227 (2018).
- [33] M. Banerjee, M. Heiblum, V. Umansky, D. E. Feldman, Y. Oreg, and A. Stern, Observation of half-integer thermal Hall conductance, *Nature (London)* **559**, 205 (2018).
- [34] Z. Wang, J. O. Rodriguez, L. Jiao, S. Howard, M. Graham, G. D. Gu, T. L. Hughes, D. K. Morr, and V. Madhavan, Evidence for dispersing 1D Majorana channels in an iron-based superconductor, *Science* **367**, 104 (2020).
- [35] J. J. He, Y. Tanaka, and N. Nagaosa, Optical responses of chiral Majorana edge states in two-dimensional topological superconductors, *Phys. Rev. Lett.* **126**, 237002 (2021).
- [36] J. J. He and N. Nagaosa, Local Raman spectroscopy of chiral Majorana edge modes in Kitaev spin liquids and topological superconductors, *Phys. Rev. B* **103**, L241109 (2021).
- [37] M. E. Barber, E. Y. Ma, and Z.-X. Shen, Microwave impedance microscopy and its application to quantum materials, *Nat. Rev. Phys.* **4**, 61 (2022).
- [38] B. A. Bernevig, *Topological Insulators and Topological Superconductors* (Princeton University Press, New Jersey, 2013).
- [39] S. B. Chung and S.-C. Zhang, Detecting the Majorana fermion surface state of ${}^3\text{He} - B$ through spin relaxation, *Phys. Rev. Lett.* **103**, 235301 (2009).
- [40] M. Sato and S. Fujimoto, Topological phases of noncentrosymmetric superconductors: Edge states, Majorana fermions, and non-Abelian statistics, *Phys. Rev. B* **79**, 094504 (2009).
- [41] Y. Nagato, S. Higashitani, and K. Nagai, Strong anisotropy in spin susceptibility of superfluid ${}^3\text{He} - B$ film caused by surface bound states, *J. Phys. Soc. Jpn.* **78**, 123603 (2009).
- [42] R. Shindou, A. Furusaki, and N. Nagaosa, Quantum impurity spin in Majorana edge fermions, *Phys. Rev. B* **82**, 180505(R) (2010).
- [43] D. C. Mattis and J. Bardeen, Theory of the anomalous skin effect in normal and superconducting metals, *Phys. Rev.* **111**, 412 (1958).
- [44] J. Ahn and N. Nagaosa, Theory of optical responses in clean multi-band superconductors, *Nat. Commun.* **12**, 1617 (2021).
- [45] B. A. Bernevig, T. L. Hughes, and S.-C. Zhang, Quantum spin Hall effect and topological phase transition in HgTe quantum wells, *Science* **314**, 1757 (2006).